Defective valvulogenesis in HB-EGF and TACE-null mice is associated with aberrant BMP signaling

Leslie F.Jackson[1,2], Ting Hu Qiu[1,3], Susan W.Sunnarborg[1], Aileen Chang[1], Chunlian Zhang[4], Cam Patterson[4] and David C.Lee[1,2,5]

[1]Department of Biochemistry & Biophysics, [2]UNC Lineberger Comprehensive Cancer Center and [4]Carolina Cardiovascular Biology Center and Department of Medicine, University of North Carolina School of Medicine, Chapel Hill, NC 27599, USA

[3]Present address: Advanced Technology Center, National Cancer Institute, Gaithersburg, MD 20892, USA

[5]Corresponding author
e-mail: dclee@med.unc.edu

Heparin-binding epidermal growth factor (HB-EGF) and betacellulin (BTC) are activating ligands for EGF receptor (EGFR/ErbB1) and ErbB4. To identify their physiological functions, we disrupted mouse *HB-EGF* and *BTC* alleles by homologous recombination. Most *HB-EGF*$^{-/-}$ mice died before weaning, and survivors had enlarged, dysfunctional hearts and reduced lifespans. Although *BTC*$^{-/-}$ mice were viable and fertile and displayed no overt defects, the lifespan of double null *HB-EGF*$^{-/-}$/*BTC*$^{-/-}$ mice was further reduced, apparently due to accelerated heart failure. *HB-EGF*$^{-/-}$ newborns had enlarged and malformed semilunar and atrioventricular heart valves, and hypoplastic, poorly differentiated lungs. Defective cardiac valvulogenesis was the result of abnormal mesenchymal cell proliferation during remodeling, and was associated with dramatic increases in activated Smad1/5/8. Consistent with the phenotype, HB-EGF transcripts were localized to endocardial cells lining the margins of wild-type valves. Similarly defective valvulogenesis was observed in newborn mice lacking EGFR and tumor necrosis factor-α converting enzyme (TACE). These results suggest that cardiac valvulogenesis is dependent on EGFR activation by TACE-derived soluble HB-EGF, and that EGFR signaling is required to regulate bone morphogenetic protein signaling in this context.

Keywords: ADAM17/betacellulin knockout/heart failure/lung/Smad

Introduction

The epidermal growth factor (EGF)–ErbB signaling network includes multiple polypeptide ligands of the EGF/neuregulin superfamily, and four related tyrosine kinase receptors, epidermal growth factor receptor (EGFR)/ErbB1–ErbB4 (reviewed by Riese and Stern, 1998). EGF-like growth factors share a conserved receptor binding motif and soluble forms are usually derived from bioactive, integral membrane precursors. Besides EGF, they include transforming growth factor α (TGFα), amphiregulin (AR), heparin-binding epidermal growth factor (HB-EGF), betacellulin (BTC), epiregulin and the recently described epigen (Strachan *et al*., 2001). These proteins all bind to EGFR/ErbB1, inducing receptor dimerization, tyrosine kinase activation and downstream signaling pathways controlling cell proliferation, differentiation, survival or motility. Heparin-binding EGF and BTC can also bind to ErbB4 (Riese *et al*., 1996a; Elenius *et al*., 1997). EGF family members vary in their ability to activate distinct ErbB heterodimers, and this may partly account for differences in their bioactivities in cell culture (Beerli and Hynes, 1996; Riese *et al*., 1996b; Graus-Porta *et al*., 1997).

Numerous actions are ascribed to the EGF family of growth factors, but their physiological functions are not well understood. Hence, our laboratory has derived mice lacking several family members individually or in combination. These studies have revealed specific roles for TGFα in patterning and function of hair follicles and migration of fetal eyelid epidermis (Luetteke *et al*., 1993), and for AR supported by EGF and TGFα in ductal morphogenesis in the developing mammary gland (Luetteke *et al*., 1999). Additionally, all three ligands are required for optimal neonatal growth, in part reflecting their roles in the mammary gland, as well as their requirement for normal development and cytoprotection of the gastrointestinal tract (Troyer *et al*., 2001). In contrast, *EGFR*$^{-/-}$ mice usually die *in utero*, although the timing is markedly affected by the genetic background (Miettinen *et al*., 1995; Sibilia and Wagner, 1995; Threadgill *et al*., 1995). However, more recent tetraploid aggregation experiments have allowed development to term (Sibilia *et al*., 1998). In comparison, the restricted or mild phenotypes of EGF family knockouts indicate that there is considerable redundancy or cooperativity in the action of these ErbB ligands.

Here we report the inactivation of mouse *HB-EGF* and *BTC*. HB-EGF was first identified as a heparin-binding mitogen for fibroblasts and smooth muscle cells that was secreted by human macrophages (Besner *et al*., 1990; Higashiyama *et al*., 1991). It is widely distributed in mammalian tissues, including skin, lung and heart (reviewed by Raab and Klagsbrun, 1997). Induced at sites of wounding, HB-EGF may also function in response to vascular injury since it is expressed in atherosclerotic plaques by aortic smooth muscle cells and other cell types (Raab and Klagsbrun, 1997), and its production by endothelial cells is induced by VEGF (Arkonac *et al*., 1998) and TNFα (Yoshizumi *et al*., 1992). Heparin-binding EGF is also implicated in uterine growth and blastocyst implantation (Kennedy *et al*., 1993; Das *et al*., 1994).

Heparin-binding EGF is derived from a bioactive, transmembrane precursor, proHB-EGF, which also functions as the diphtheria toxin receptor in primates (Naglich *et al*., 1992). ProHB-EGF interacts with tetraspanin and other membrane proteins, and may distinctively signal growth inhibition or apoptosis rather than the proliferative response induced by soluble HB-EGF (reviewed by Iwamoto and Mekada, 2000). In this light, the identity of the protease that regulates HB-EGF shedding is an important topic that has assumed additional significance because regulated release of soluble HB-EGF contributes to transactivation of EGFR by G-protein-coupled receptors (GPCR) (Prenzel *et al*., 1999). Several metalloproteases, including members of the A Disintegrin and Metalloprotease (ADAM) (Izumi *et al*., 1998; Asakura *et al*., 2002; Lemjabbar and Basbaum, 2002; Yan *et al*., 2002) and matrix metalloprotease (MMP) (Suzuki *et al*., 1997; Bursi *et al*., 2002; Yu *et al*., 2002) families, have been identified as putative proHB-EGF convertases.

BTC was identified as a mitogen secreted by pancreatic β-cell insulinomas (Sasada *et al*., 1993; Shing *et al*., 1993) and it is implicated in the normal development and function of the pancreas (reviewed in Dunbar and Goddard, 2000). It is highly expressed in fetal pancreas, promotes islet growth (Demeterco *et al*., 2000) and co-regulates differentiation of insulin-producing cells (Mashima *et al*., 1996, 1999). It also promotes β-cell neogenesis and improves glucose tolerance in a mouse model of diabetes (Yamamoto *et al*., 2000). However, BTC is also widely expressed and additional roles in blastocyst implantation (Das *et al*., 1997), gastrointestinal function (Kallincos *et al*., 2000) and atherosclerosis (Tamura *et al*., 2001) have been proposed.

We report here that *HB-EGF*$^{-/-}$ and *BTC*$^{-/-}$ mice are viable and fertile, but *HB-EGF*$^{-/-}$ mice have severely shortened lifespans and exhibit specific cardiac and lung defects. These phenotypes are mimicked in mice lacking either EGFR or tumor necrosis factor-α converting enzyme (TACE), providing genetic evidence that these proteins are the relevant ErbB receptor and HB-EGF convertase, respectively.

Results

HB-EGF$^{-/-}$ *and BTC*$^{-/-}$ *mice are viable and fertile*

Mouse *HB-EGF* and *BTC* were disrupted in embryonic stem cells by homologous recombination (Figure 1A). *HB-EGF* exons 1 and 2 were replaced with PGK-*Neo*, thus deleting the signal peptide and propeptide, and simultaneously inducing a frameshift to prevent translational read through. *BTC* was inactivated by eliminating exon 3, which encodes the first two loops of the EGF-like sequence that are critical for receptor binding. Lines of *HB-EGF*$^{-/-}$ and *BTC*$^{-/-}$ mice were established from targeted ES clones on a mixed C57BL/6J × 129 background, and the desired targeting events verified by Southern blots of genomic DNA (Figure 1B) and exon-specific PCR (Figure 1C). Northern blots confirmed the absence of the respective transcripts (Figure 1D).

The average litter size from intercrosses of *HB-EGF*$^{+/-}$ mice was 10.2 (n = 13 litters, 132 pups), a typical size for our colony. However, 12 neonates died in the first week after birth and genotyping of the remaining 120 pups at weaning revealed a non-Mendelian distribution of genotypes: 28%$^{+/+}$, 62%$^{+/-}$ and 11%$^{-/-}$. Surviving *HB-EGF*$^{-/-}$ mice grew normally, were fertile and matings between them produced litters of typical size at birth, suggesting there was little to no intrauterine loss of HB-EGF$^{-/-}$ mice. However, only 40% of the *HB-EGF*$^{-/-}$ offspring survived to weaning (n = 7 litters, 20/50 pups survived) compared with >80% of control pups (n = 5 litters, 32/39 pups survived), reminiscent of the results of *HB-EGF*$^{+/-}$ matings. Mammary gland morphology was normal in *HB-EGF*$^{-/-}$ dams, and there was no functional evidence of impaired lactation. Gastrointestinal tract architecture was also normal in *HB-EGF*$^{-/-}$ neonates, and the body weights of surviving *HB-EGF*$^{-/-}$ pups were within normal range from 1 to 3 weeks of age (data not shown). Thus, increased mortality of *HB-EGF*$^{-/-}$ mice was not ascribed to defects in nursing or nutrient absorption.

Matings between *BTC*$^{+/-}$ parents produced offspring in the expected Mendelian ratios (18%$^{+/+}$, 56%$^{+/-}$, 26%$^{-/-}$; n = 14 litters) at weaning and *BTC*$^{-/-}$ mice were viable and grew normally. Matings between homozygous *BTC*$^{-/-}$ mice also yielded normal sized litters. Since BTC is implicated in the growth and development of the pancreas (Dunbar and Goddard, 2000), we specifically examined this tissue. No morphological differences were observed in newborn pancreata, and adult *BTC*$^{+/+}$ and *BTC*$^{-/-}$ males responded similarly to a glucose challenge test (data not shown). Also, expression of insulin, glucagon, cytokeratin and amylase were normal in *BTC*$^{-/-}$ pancreata (P.Miettinen, personal communication).

Defective cardiac valvulogenesis in HB-EGF$^{-/-}$ *mice*

Examination of newborn hearts revealed grossly enlarged and stenotic semilunar (SL) (aortic and pulmonary) and atrioventricular (AV) valves in all newborn *HB-EGF*$^{-/-}$ mice (n = 14) compared with *HB-EGF*$^{+/+}$ mice (n = 10) (Figure 2A–F). For example, the mean area of *HB-EGF*$^{-/-}$ aortic valves (Figure 2M) was 56.7 ± 17 mm^2 (n = 7) compared with 21.9 ± 4.6 mm^2 (n = 5) for *HB-EGF*$^{+/+}$ controls (P = 0.0025).

Enlarged SL, but not AV, valves were observed in *waved-2* (*EGFR*$^{wa\text{-}2/wa\text{-}2}$) mice, which encode a kinase-impaired EGFR mutant, and in *EGFR*$^{-/-}$ mice (Chen *et al*., 2000). We examined *EGFR*$^{wa\text{-}2/wa\text{-}2}$ hearts and confirmed that only SL valves were enlarged (data not shown). However, both SL and AV valves were dramatically enlarged in *EGFR*$^{-/-}$ hearts (Figure 2G–I). Thus, aortic valve area in four *EGFR*$^{-/-}$ hearts was 56.6 ± 15.4 mm^2 compared with 16.7 ± 4.5 mm^2 in four control hearts (P = 0.0286) (Figure 2M). We attribute the difference between the two models to residual signaling by the wa-2 receptor and a lower threshold requirement in SL valves. Abnormal valves were not observed in triple null mice lacking AR, EGF and TGFα (Chen *et al*., 2000), nor in *BTC*$^{-/-}$ hearts (data not shown). Collectively, these results indicate that HB-EGF is uniquely required as an EGFR ligand for cardiac valvulogenesis.

TACE$^{-/-}$ *mice display identical heart valve defects*

ADAM17/TACE is required for conversion of membrane-anchored proTGFα to the soluble ligand (Peschon *et al*., 1998; Sunnarborg *et al*., 2002). *TACE*$^{-/-}$ mice displayed generalized epithelial defects reminiscent of those

observed in *EGFR*$^{-/-}$ animals, and we showed in cell-based and *in vitro* peptide assays that TACE promotes HB-EGF processing (Sunnarborg *et al*., 2002). To assess whether TACE functions as an HB-EGF convertase *in vivo*, we examined the heart valves of newborn TACE-null mice. Hearts from these mice had SL and AV valves that were similarly enlarged compared with *HB-EGF*$^{-/-}$ and *EGFR*$^{-/-}$ counterparts (Figure 2J–L), e.g. the mean area of *TACE*$^{-/-}$ aortic valves was 57.5 ± 29.4 mm^2 compared with 20.0 ± 7.4 mm^2 for *TACE*$^{+/+}$ controls (n = 4 each genotype; P = 0.0079) (Figure 2M).

Highly localized expression of HB-EGF in valves

We examined HB-EGF expression in control hearts during cardiac valve development, from E11.5 through E15.5.

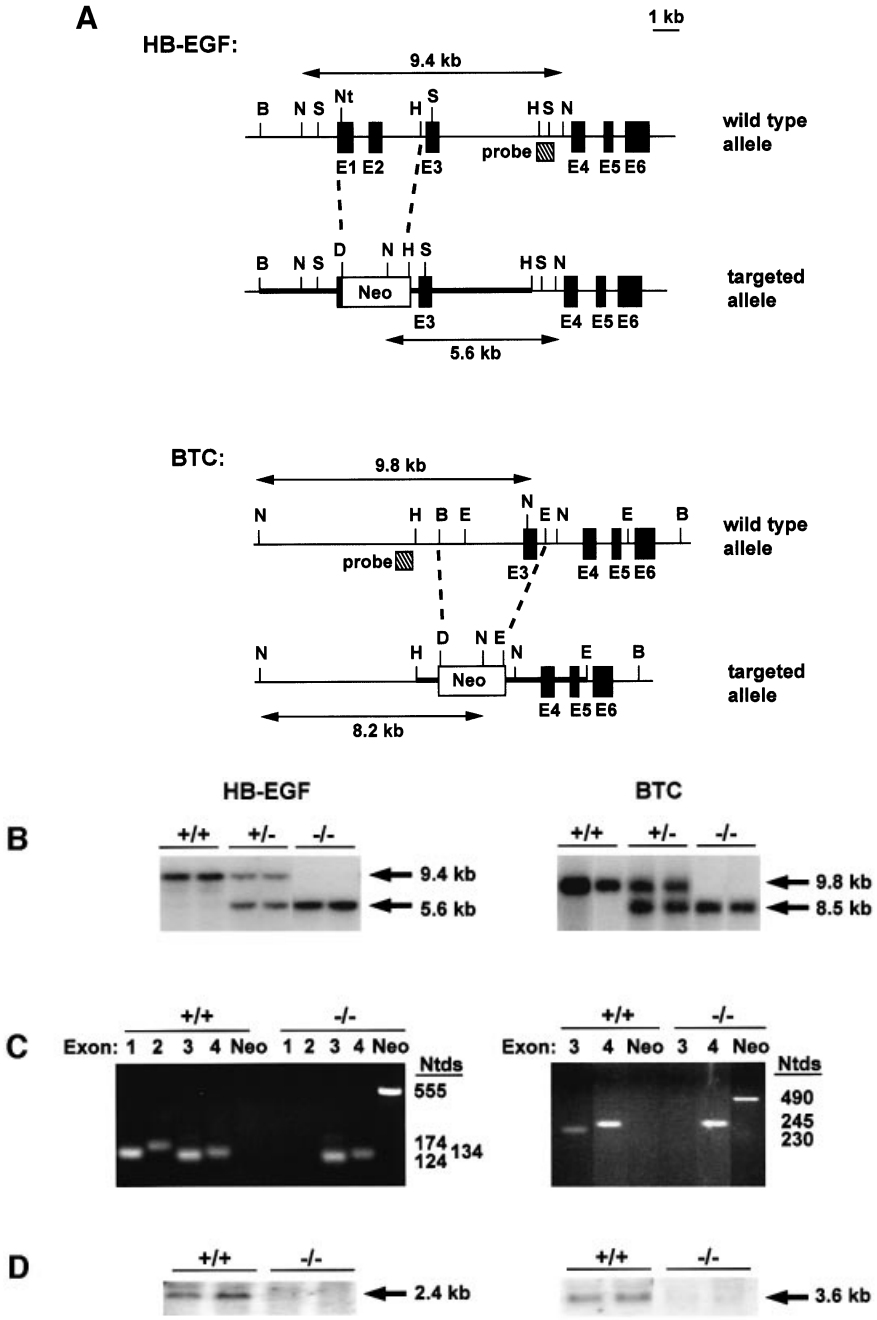

Fig. 1. Targeted disruption of *HB-EGF* and *BTC*. (**A**) Schematics illustrate strategies used to inactivate the mouse *HB-EGF* and *BTC* alleles. Targeting constructs were designed to eliminate exons (filled boxes) 1 and 2 of the *HB-EGF* gene, or exon 3 of the *BTC* gene using genomic sequences isolated from a mouse 129/Sv library. Heavy lines denote 5′ and 3′ arms of homology, and dashed lines bracket the genomic regions replaced by the *Neo* cassette. Hatched boxes mark probes used to verify correct targeting, and the locations of useful restriction sites and resulting fragments are noted. B, *Bgl*II; E, *EcoR*I; H, *Hin*dIII; N, *Nco*I; Nt, *Not*I; S, *Stu*I. (**B**) Southern blot analyses of genomic DNAs digested with *Nco*I, showing results diagnostic for wild-type, heterozygous and homozygous targeted alleles using the indicated probes. (**C**) Genomic PCR using exon- or Neo-specific primers. (**D**) Northern blots of lung RNA from mice of the designated genotypes. Arrows indicate the apparent mass of DNA or RNA species. Ntds, nucleotides; kb, kilobases.

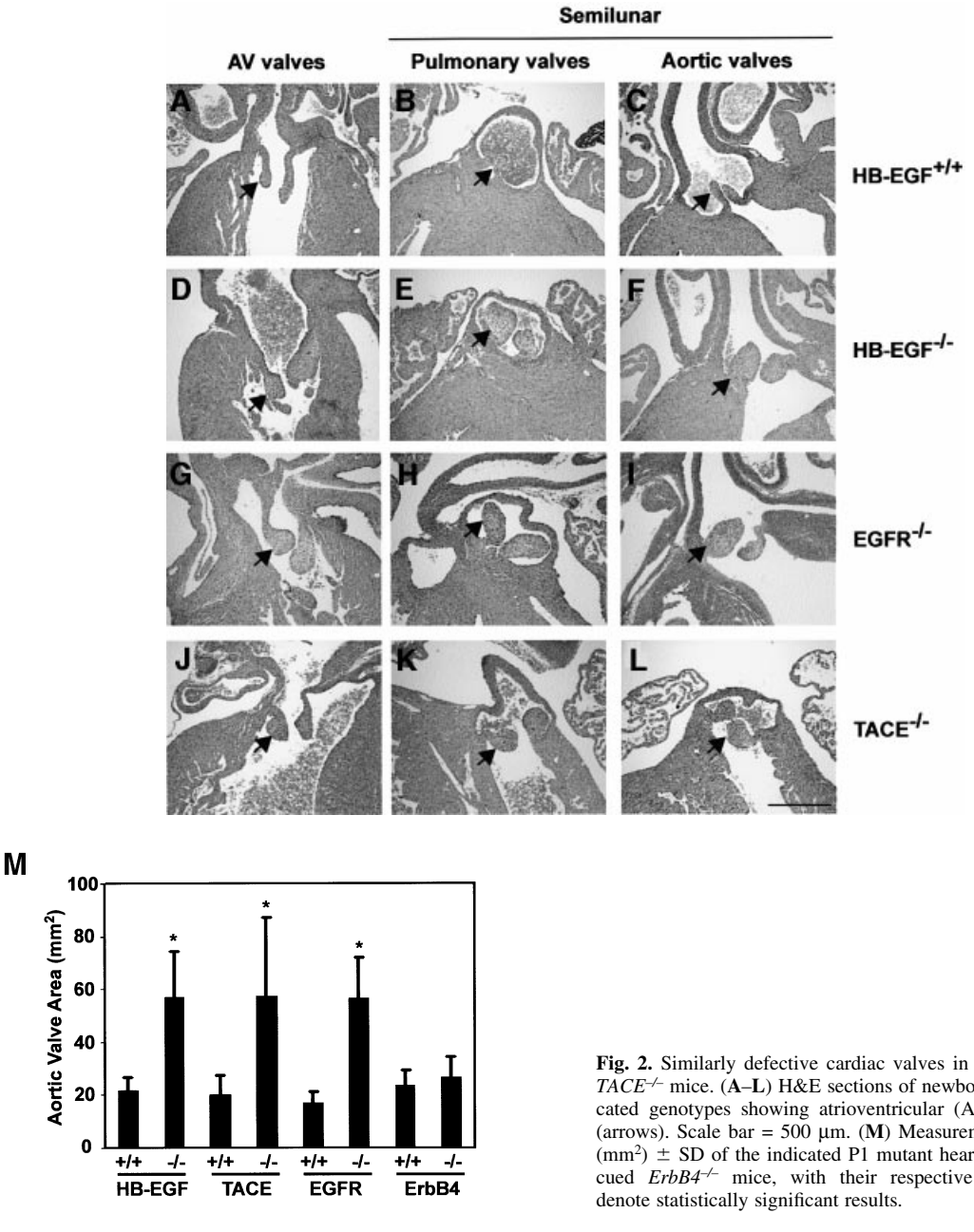

Fig. 2. Similarly defective cardiac valves in *HB-EGF*$^{-/-}$, *EGFR*$^{-/-}$ and *TACE*$^{-/-}$ mice. (**A–L**) H&E sections of newborn (P1) hearts of the indicated genotypes showing atrioventricular (AV) and semilunar valves (arrows). Scale bar = 500 μm. (**M**) Measurement of aortic valve areas (mm^2) ± SD of the indicated P1 mutant hearts, including those of rescued *ErbB4*$^{-/-}$ mice, with their respective +/+ controls. Asterisks denote statistically significant results.

HB-EGF transcripts were highly localized to the endocardial cells lining the margins of AV and SL (both aortic and pulmonary) valves, as shown at E14.5 (Figure 3A–F). Diffuse expression was also apparent throughout the myocardium, especially at later times (data not shown). EGFR transcripts were detected throughout the heart, including in developing valves, but enriched in the endocardial cushion, as shown for E14.5 (Figure 3G and H). TACE transcripts were found throughout the heart at this same developmental stage (Figure 3M and N), including in HB-EGF-expressing cells at the margins of AV and SL valves. Immunohistochemistry confirmed broad distribution of TACE protein (data not shown). Thus, growth factor, receptor and convertase are all coexpressed, consistent with the phenotypic similarities.

Since HB-EGF binds to ErbB4 as well as EGFR, we considered that ErbB4 might transduce HB-EGF signals required for valvulogenesis. *ErbB4* transcripts were detected throughout the developing heart, including in cushions and valves, as shown at E14.5 in Figure 3K and L. This contrasts with restricted expression in the ventricular myocardium at E10.5 (Gassmann *et al*., 1995). Since *ErbB4*$^{-/-}$ embryos die early in gestation with defects in ventricular trabeculation, it was not possible to examine valvulogenesis in these mice. However, the knockout has recently been rescued by introduction of an *ErbB4* transgene in heart muscle under the control of the α-myosin heavy chain promoter, which directs expression specifically to cardiomyocytes (Tidcombe *et al*., 2001). We examined SL and AV valves in these transgenic mice and found them to be of normal

size (Figure 2M), suggesting that ErbB4 is not required for valvulogenesis. However, we cannot exclude possible low level expression of the transgene in valve mesenchyme sufficient to direct normal valvulogenesis.

We also observed *ErbB3* transcripts in the cushions and valves from E12.5 to 15.5 (Figure 3I and J), as previously shown for earlier time points (Meyer and Birchmeier, 1995). Thus, ErbB3 could potentially influence HB-EGF signaling through heterodimerization with EGFR.

Remodeling of valves requires HB-EGF

To address the mechanism of HB-EGF action, we compared valve development in *HB-EGF*$^{-/-}$ and *HB-EGF*$^{+/+}$ hearts from E12.5 to E15.5. Immature valves (AV and PV) were comparably sized at E12.5 and E13.5 in both genotypes, indicating that early events in valve formation occurred normally without HB-EGF. However, subsequent remodeling of valves was clearly perturbed. Whereas large, immature AV (Figure 4A and B) and PV (Figure 4E and F) valves of control hearts were remodeled to form slender valve leaflets, *HB-EGF*$^{-/-}$ valves remained enlarged throughout the period (Figure 4C, D, G and H). The largest size reduction for *HB-EGF*$^{+/+}$ AV valves occurred from E13.5 to E14.5, and for PV valves from E12.5 to E13.5 (Figure 4Q and R). In contrast, *HB-EGF*$^{-/-}$ valves were only modestly reduced in size, remaining 36–46% larger than the control counterparts through E15.5, differences that were significant ($P = 0.0286$) for AV valves at both time points and for PV valves at E15.5.

Impaired remodeling of *HB-EGF*$^{-/-}$ valves could be due to reduced cellular apoptosis or increased cellular proliferation. TUNEL assays revealed no differences in the percentage of cells undergoing apoptosis in *HB-EGF*$^{+/+}$ versus *HB-EGF*$^{-/-}$ valves at E14.5 or E15.5 (Figure 4S). In contrast, the percentages of bromodeoxyuridine (BrdU)-positive cells were significantly ($P = 0.0286$) increased ~3.5-fold in AV valves and ~2-fold in PV valves of *HB-EGF*$^{-/-}$ hearts at E14.5 (Figure 4T). There was no change in the distribution of BrdU-positive cells in *HB-EGF*$^{-/-}$ valves, which were found throughout the valve mesenchyme. Thus, surprisingly, impaired remodeling of *HB-EGF*$^{-/-}$ valves was due to excessive proliferation of mesenchymal cells. Since the cardiac valves of young *HB-EGF*$^{-/-}$ adults were even larger and more disfigured than comparable controls (data not shown), we speculate that cellular proliferation continues beyond the embryonic time points analyzed here.

To determine whether the enlarged cardiac valves of newborn *EGFR*$^{-/-}$ and *TACE*$^{-/-}$ mice had a similar origin, we examined the respective hearts at E15.5. For both genotypes, AV and PV valves were significantly enlarged compared with controls, suggesting that impaired remodeling was also the cause of valve enlargement in these mutants (Figure 4I–P).

Bone morphogenetic protein (BMP) signaling is disregulated in the absence of HB-EGF

A clue to the mechanism of defective valvulogenesis came from an initial gene array comparison performed with total E14.5 *HB-EGF*$^{+/+}$ and *HB-EGF*$^{-/-}$ hearts. The three genes most strongly upregulated in mutant heart, *dHAND*, *Smad6* and *Id-1* (data not shown), are all implicated in BMP signaling, which is required for outflow tract septation and valve development (Kim *et al.*, 2001;

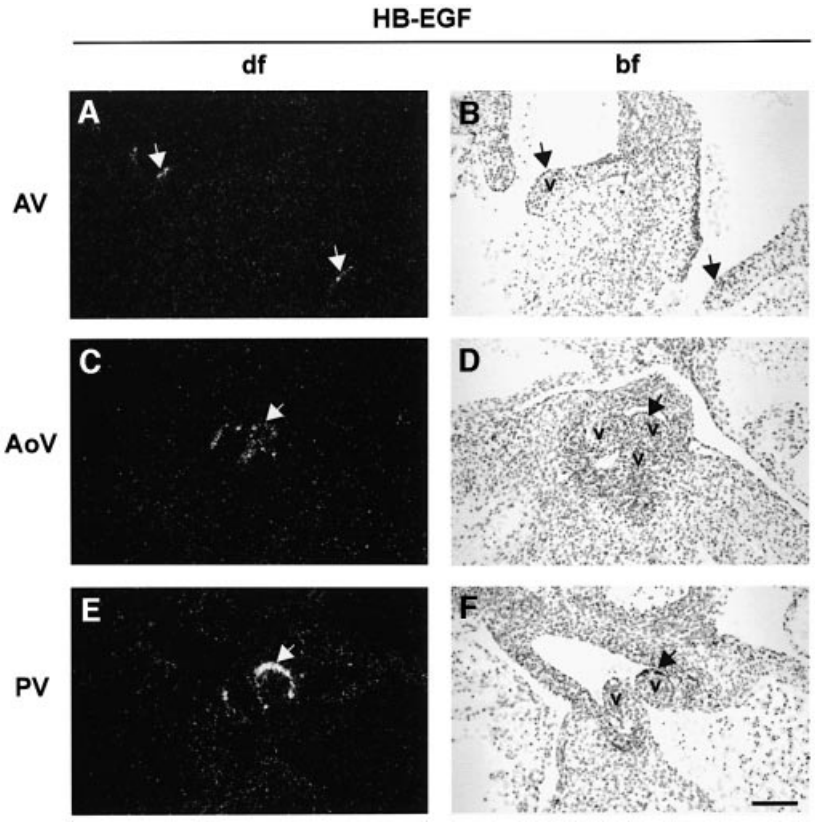

Gaussin *et al*., 2002; Delot *et al*., 2003). Since *Smad6*$^{-/-}$ mice have hyperplastic valves (Galvin *et al*., 2000) similar to those observed here, presumably due to disregulated BMP signaling in the absence of this inhibitor Smad, and cell culture studies have established the potential for EGFR inhibition of BMP signaling (Kretzschmar *et al*., 1997; Nonaka *et al*., 1999), we speculated that defective valvulogenesis in our mice could be due to loss of BMP regulation. To test this, we examined activation of Smad1/5/8 in sections of *HB-EGF*$^{+/+}$ and *HB-EGF*$^{-/-}$ hearts using an antibody that detects phosphorylated forms of these BMP signaling effectors. Figure 5 reveals dramatically higher numbers of cells staining positive for nuclear phospho-Smad1/5/8 in pulmonary and aortic valves of mutant hearts compared with the control tissues at E14.5. A similar, albeit less dramatic, trend was seen in AV valves (data not shown). In contrast, *HB-EGF*$^{+/+}$ and *HB-EGF*$^{-/-}$ valves showed similarly high levels of activated Smad1/5/8 in AV and aortic valves at E12.5 during the proliferative phase of valve development (data not shown).

HB-EGF$^{-/-}$ *hearts are enlarged and dysfunctional*

An unusually high proportion (43%) of *HB-EGF*$^{-/-}$ adult males and females died within the first year of life. At necropsy, these mice were found to have enlarged hearts and congested lungs, with no other apparent pathological defects. A systematic comparison showed that the heart-to-body weight ratios of male *HB-EGF*$^{-/-}$ mice increased continuously from birth through 6 months of age compared with wild-type controls, although the largest relative increase occurred between 3 and 6 weeks of age (data not shown). Examples of enlarged hearts of apparently healthy, 6-week-old male *HB-EGF*$^{-/-}$ mice are shown in Figure 6A–C. The mean heart-to-body weight ratio for 6-week-old *HB-EGF*$^{-/-}$ mice was 1.27 $\pm$ 0.20% compared with 0.80 $\pm$ 0.03% for *HB-EGF*$^{+/+}$ controls (n = 5 both genotypes; P = 0.0079). At this stage, ventricular myocyte size (Figure 6D and E) and number per unit area were not significantly different between the two genotypes, indicating that enlargement was due to hypercellularity. However, we did not observe significant incorporation of BrdU into 5-week-old hearts of either genotype, suggest-

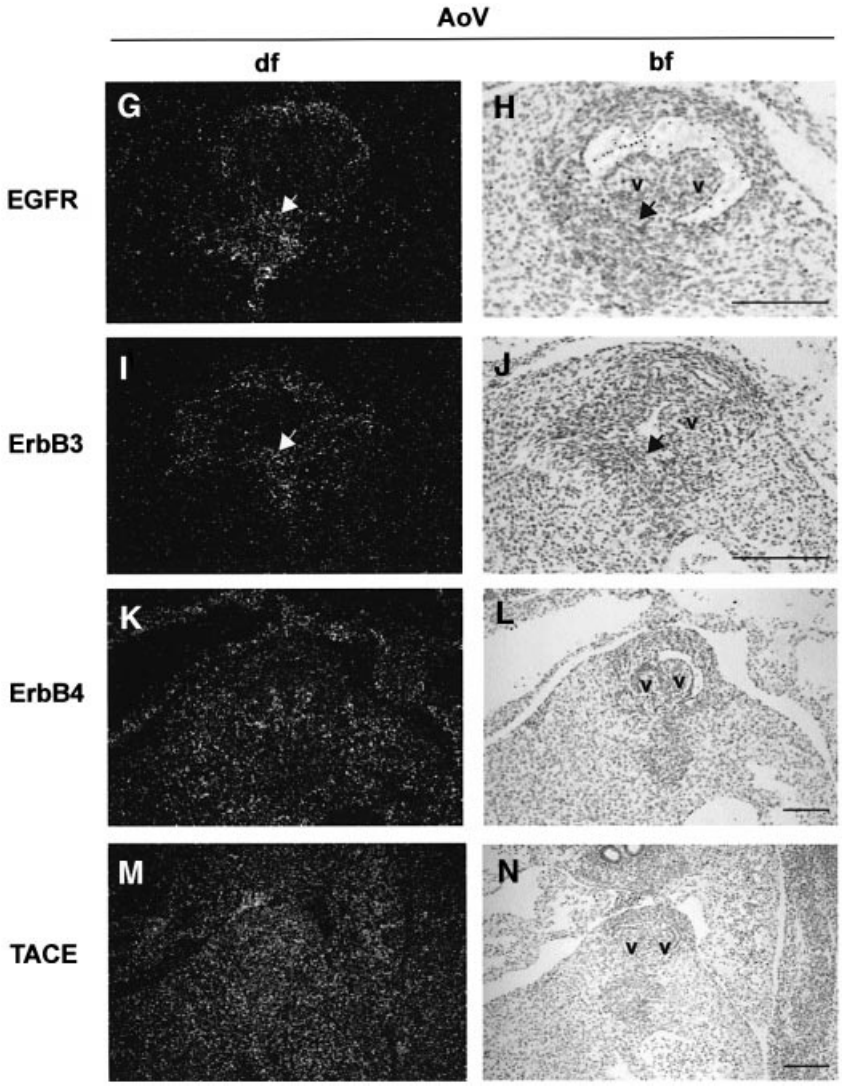

Fig. 3. *In situ* detection of *HB-EGF*, *EGFR*, *ErbB3*, *ErbB4* and *TACE* transcripts in wild-type cardiac valves. (**A**–**F**) *HB-EGF*; (**G** and **H**) *EGFR*; (**I** and **J**) *ErbB3*; (**K** and **L**) *ErbB4*; (**M** and **N**) *TACE*. Arrows mark regions of high expression. Sense riboprobes were hybridized to confirm specific hybridization in each case (data not shown). AoV, aortic valve; bf, bright field; df, dark field; v, valves. Scale bars = 100 μm.

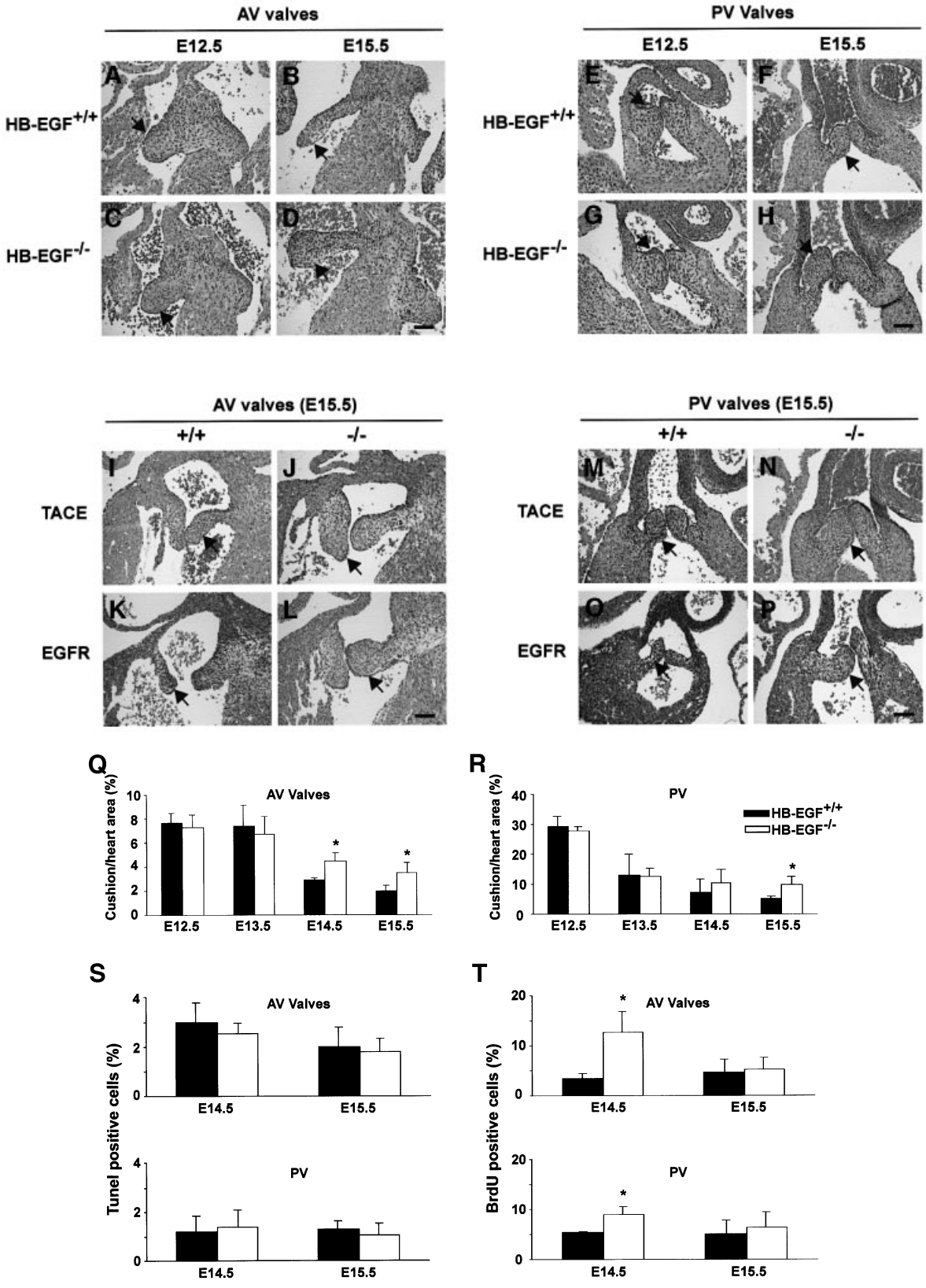

Fig. 4. Defective remodeling of cardiac valves in mutant mouse hearts. (A–H) H&E sections of *HB-EGF*$^{+/+}$ or *HB-EGF*$^{-/-}$ hearts showing (**A**–**D**) atrioventricular (AV) valves or (**E**–**H**) pulmonary valves (PV) at the indicated time points. (**I**–**P**) H&E sections of heart showing AV valves or PV valves of the indicated *TACE* or *EGFR* genotypes at E15.5. Arrows denote valves. Scale bars = 100 μm. (Q–T) Quantitative comparison of valvulogenesis in *HB-EGF*$^{+/+}$ or *HB-EGF*$^{-/-}$ hearts. (**Q** and **R**) Cushion/heart ratio ± SD at the indicated ages. (**S**) Percentage of TUNEL-positive cells at the indicated ages in AV valves or PV; (**T**) percentage of BrdU-positive cells. Filled bars, *HB-EGF*$^{+/+}$; unfilled bars, *HB-EGF*$^{-/-}$. Asterisks denote statistically significant results.

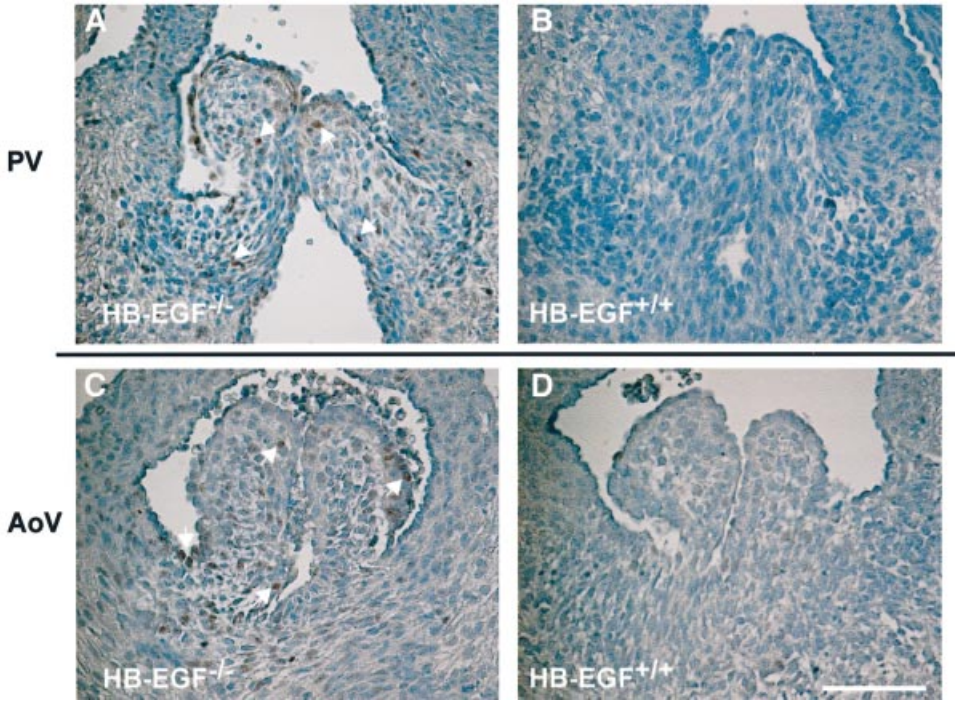

Fig. 5. Disregulated Smad signaling in HB-EGF mutant cushions. Sections of (**A** and **B**) pulmonary valve (PV) or (**C** and **D**) aortic valve (AoV) from E14.5 immunostained with phospho-Smad1/5/8 antibody and counterstained with hematoxylin. Arrows mark positive staining cells. Scale bar = 100 μM.

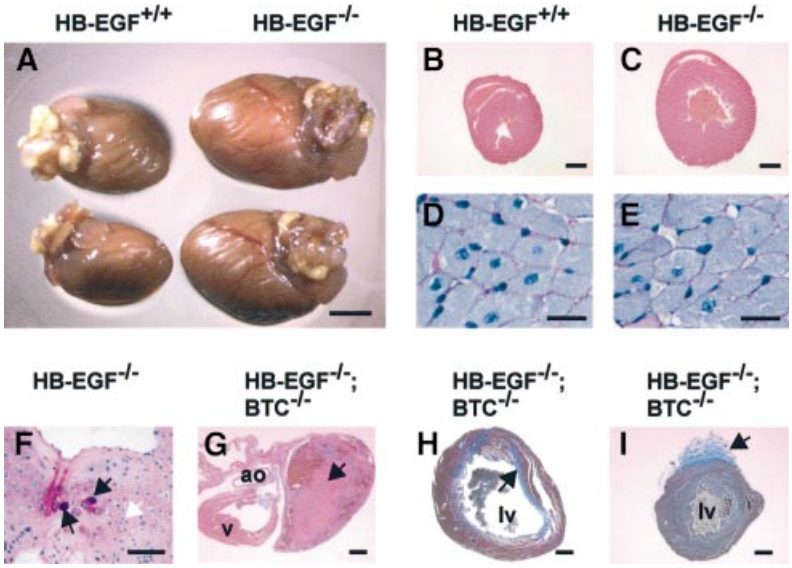

Fig. 6. Cardiac defects in *HB-EGF*$^{-/-}$ and *HB-EGF*$^{-/-}$*/BTC*$^{-/-}$ mice. (**A**) Hearts from 6-week-old male mice. (**B** and **C**) H&E-stained cross-sections of 6-week-old (B) *HB-EGF*$^{+/+}$ and (C) *HB-EGF*$^{-/-}$ hearts. (**D** and **E**) PAS-stained transverse sections of left ventricle cardiomyocytes. (**F**) PAS-stained section of thickened aortic valve leaflet from 6-month-old *HB-EGF*$^{-/-}$ heart. White arrow marks chondrocytes; black arrows denote ectopic cartilage formation. (**G**) H&E-stained section of *HB-EGF*$^{-/-}$*/BTC*$^{-/-}$ heart. Arrow marks a thrombus in the left atrium. (**H** and **I**) Masson trichrome-stained sections of *HB-EGF*$^{-/-}$*/BTC*$^{-/-}$ hearts. Arrows mark extensive intraventricular (H) or focal epicardial (I) fibrosis (blue stain) within or on the left ventricle. v, ventricle; ao, aorta; lv, left ventricle. Scale bars = 3.5 mm (A), 1 mm (B and C), 20 μm (D and E), 100 μm (F), 1 mm (G–I).

ing that proliferation occurred gradually. A comparison of transverse sections from 6-month-old male mice indicated that further heart enlargement included a significant hypertrophic component.

To assess the functionality of *HB-EGF*$^{-/-}$ hearts, we performed non-invasive transthoracic echocardiography (ECG) on 5-month-old mice. Left ventricular end-diastolic and -systolic dimensions were significantly larger, confirming cardiomegaly (Table I). Calculations of fractional shortening (SF%) revealed significant systolic dysfunction in *HB-EGF*$^{-/-}$ mice, which may be observed in advanced human aortic valve disease (although a myopathic contribution to the ECG observations cannot be excluded). Aortic dilation, a classic symptom of valvular stenosis, was also observed in ECGs (data not shown).

Histological sections of hearts from similarly aged *HB-EGF*$^{-/-}$ mice showed grossly enlarged and deformed valves, and confirmed aortic dilation. Chondrocytes and

Table I. Echocardiogram results for *HB-EGF* and *HB-EGF/BTC* mice

Genotype	BW (g)	HR (b.p.m.)	IVST (mm)	LVEDD (mm)	LVESD (mm)	PWT (mm)	SF (%)
HB-EGF$^{+/+}$	38.4 ± 3.9	659 ± 55	0.08 ± 0.03	0.32 ± 0.03	0.10 ± 0.02	0.1 ± 0.01	68.7 ± 2.7
HB-EGF$^{-/-}$	35.3 ± 2.3	668 ± 21	0.10 ± 0.03	0.41 ± 0.05*	0.20 ± 0.05*	0.1 ± 0.02	51.6 ± 7.4*
HB-EGF$^{+/+}$/*BTC*$^{+/+}$	33.6 ± 2.8	653 ± 55	0.07 ± 0.01	0.30 ± 0.02	0.08 ± 0.01	0.07 ± 0.01	71.8 ± 3.3
HB-EGF$^{-/-}$/*BTC*$^{-/-}$	29.0 ± 2.5*	695 ± 43	0.07 ± 0.01	0.39 ± 0.08*	0.17 ± 0.10*	0.09 ± 0.01	58.8 ± 15.9*

Non-invasive transthoracic echocardiography was performed on unanesthetized, male mice. Values are mean ± SD for 5-month-old *HB-EGF*$^{+/+}$ (n = 5) and *HB-EGF*$^{-/-}$ (n = 5) mice, and 4-month-old *HB-EGF*$^{+/+}$/*BTC*$^{+/+}$ (n = 6) and *HB-EGF*$^{-/-}$/*BTC*$^{-/-}$ (n = 6) mice. BW, body weight; HR, heart rate; IVST, interventricular septal distance; LVEDD, left ventricular end-diastolic dimension; LVESD, left ventricular end-systolic dimension; PWT, posterior wall thickness; SF, fractional shortening. Asterisks denote values significantly different from respective wild-type controls ($P < 0.05$).

ectopic cartilage formation were observed throughout the aortic valve leaflets of *HB-EGF*$^{-/-}$ but not control hearts (Figure 6F), possibly as a consequence of disregulated BMP signaling in *HB-EGF*$^{-/-}$ hearts. Cartilaginous metaplasia and ossification within the outflow tracts of the heart were observed in *Smad6*$^{-/-}$ mice (Galvin *et al*., 2000), and in the cardiac valves of patients undergoing valve replacement (Mohler *et al*., 2001).

Combined loss of BTC exacerbates heart defects

We interbred *HB-EGF*$^{-/-}$ and *BTC*$^{-/-}$ mice to generate double nulls in order to explore redundancy or cooperativity between these two EGFR/ErbB4 binding ligands. *HB-EGF*$^{-/-}$/*BTC*$^{-/-}$ double null mice were viable and fertile, but displayed a significantly higher rate of mortality. Most (54%) were dead by 4 months of age, and 83% (n = 24) had died within the first year. As expected, cardiac valves of *HB-EGF*$^{-/-}$/*BTC*$^{-/-}$ newborns were enlarged; however, the mean aortic valve area of newborn *HB-EGF*$^{-/-}$/*BTC*$^{-/-}$ mice (55.8 ± 8.4 mm^2) was not significantly different from that of *HB-EGF*$^{-/-}$ mice (compare with values in Figure 2M). Electrocardiograms of 4-month-old *HB-EGF*$^{-/-}$/*BTC*$^{-/-}$ mice confirmed cardiomegaly and systolic dysfunction compared with age-matched controls (Table I). However, adult *HB-EGF*$^{-/-}$/*BTC*$^{-/-}$ mice displayed certain cardiac defects rarely or never seen in *HB-EGF*$^{-/-}$ mice. Left atrial dilation and thrombosis (see the clot in Figure 6G), as well as marked fibrosis within and on the left ventricle near the apex were commonly observed ante mortem in moribund *HB-EGF*$^{-/-}$/*BTC*$^{-/-}$ mice from 2 months of age (Figure 6H and I). We speculate that surface fibrosis may have resulted from friction between the *HB-EGF*$^{-/-}$/*BTC*$^{-/-}$ heart and the pericardium, possibly due to ventricular dilation (Figure 6H) during end-stage heart failure. None of these defects was observed in *BTC*$^{-/-}$ hearts. Ectopic cartilage formation observed in *HB-EGF*$^{-/-}$ hearts was also observed in *HB-EGF*$^{-/-}$/*BTC*$^{-/-}$ mice, but not in *BTC*$^{-/-}$ hearts (data not shown). Double null mice lacking HB-EGF and AR were also generated, but did not display aggravated heart defects or reduced lifespans relative to *HB-EGF*$^{-/-}$ mice (data not shown).

Morphological defects and alveolar immaturity in HB-EGF$^{-/-}$ lungs

We observed defects in the lungs in ~50% of *HB-EGF*$^{-/-}$ newborns. Mesenchymal tissue between alveoli was abnormally thickened compared with wild-type tissue (Figure 7A and B), and *HB-EGF*$^{-/-}$ lungs (n = 9) contained significantly fewer alveoli than *HB-EGF*$^{+/+}$ tissue (n = 6): 39.2 ± 4.0 versus 28.1 ± 6.7 per field (P = 0.0012) (Figure 7G). These defects, which are consistent with HB-EGF expression in this tissue, were most striking in pups that were clearly in distress (no milk in the stomach, little movement), suggesting they may have contributed to the mortality of *HB-EGF*$^{-/-}$ pups. PAS staining revealed a much higher fraction of immature, glycogen-containing cells in newborn *HB-EGF*$^{-/-}$ lungs compared with controls (Figure 7C and D); conversely, fewer cells in *HB-EGF*$^{-/-}$ lungs stained positive for the type II pneumocyte marker, pro-surfactant C (Figure 7E and F). Similar defects have been noted in *EGFR*$^{-/-}$ (Miettinen *et al*., 1995, 1997) and *TACE*$^{-/-}$ lungs (Zhao *et al*., 2001), providing further evidence of a link between TACE and HB-EGF–EGFR signaling.

Discussion

Human heart valve defects are the most common type of congenital heart disease (CHD) (Bartram *et al*., 2001). Heart valves develop from endocardial cushions, which form when endothelial cells in the AV and outflow tract areas undergo an epithelial-to-mesenchymal transformation and invade the adjacent acellular matrix. The cells then proliferate to form cushions that subsequently give rise to the septa of the four-chambered heart as well as the cardiac valves (Eisenberg and Markwald, 1995; Lamers *et al*., 1995). In the mouse, endocardial cushion formation is complete by E12.5 (Lakkis and Epstein, 1998) and is followed by cellular apoptosis and differentiation, which remodel the cushions to slender valve leaflets. In mice lacking either HB-EGF or EGFR, valvulogenesis is disrupted, leading to thickened, stenotic valves. Thus, our findings corroborate a role for EGFR in valvulogenesis (Chen *et al*., 2000), extend this requirement to AV valves and establish that HB-EGF is uniquely required to activate EGFR ligand in this context.

Valvulogenesis is a complex process (Srivastava and Olson, 2000), and hence we considered various possible explanations for the *HB-EGF*$^{-/-}$ phenotype, including altered homing or migration of neural crest-derived cells. However, it is unlikely that the phenotype is due to aberrant neural crest cell migration since cushion formation, which also depends on this process, occurred normally. In addition, defects involving neural crest cells are typically associated with cardiac septal defects (Chien, 2000), and these are not observed in our mice. Finally, recent evidence suggests that neural crest cells do not

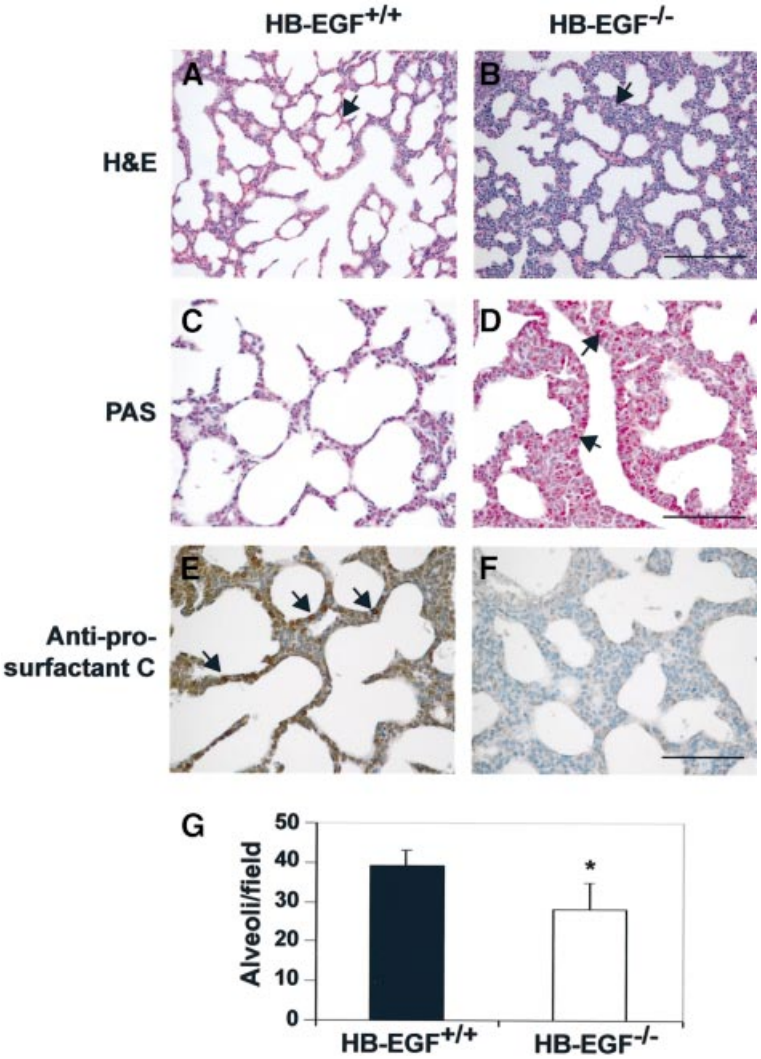

Fig. 7. A comparison of lung morphology and maturity in *HB-EGF*$^{+/+}$ and *HB-EGF*$^{-/-}$ mice. (**A** and **B**) H&E-stained sections of newborn lungs. Arrows point to thickened mesenchyme. (**C** and **D**) PAS-stained sections of newborn lung. Arrows (D) point to areas enriched in cells with high glycogen content. (**E** and **F**) Sections of newborn lung immunostained for prosurfactant C. Arrows point to positive cells. (**G**) Bars indicate mean number of alveoli counted from duplicate histological sections of newborn lung (n = 6–9 mice) of the indicated genotypes ± SD. Asterisk denotes significant result (P = 0.0012). Scale bars = 200 μm (A and B), 100 μm (C–F).

contribute to AV valves (Jiang *et al*., 2000), which are similarly enlarged in our mice. Alternatively, we speculated that loss of the HB-EGF precursor, which selectively induced cellular apoptosis rather than proliferation in cell culture (Iwamoto *et al*., 1999), might reduce or eliminate cell death required for remodeling of the cardiac valves. However, the rate of apoptosis was unchanged in *HB-EGF*$^{-/-}$ valves during remodeling. Instead, our results indicate that the phenotype is due to excessive or unscheduled proliferation in the absence of HB-EGF, a surprising finding.

A possible clue to the mechanism of HB-EGF/EGFR action came from substantial evidence that cardiac valve formation depends on signaling by BMPs, members of the TGFβ superfamily. For example, mice encoding a genetically modified BMP2 receptor (BMP2R) with reduced signaling capacity displayed conspicuous defects in the outflow tract of the heart. These included a lack of conotruncal septation below the valves, interruption of the aortic arch and a deficiency of SL valves (Delot *et al*., 2003). Similarly, double null mice lacking both BMP6 and BMP7, as well as mice deficient in Tolloid, a homolog of the *Drosophila* metalloprotease that cleaves the BMP antagonist, Chordin, also had hypoplastic valves (Clark *et al*., 1999; Kim *et al*., 2001). On the other hand, mice lacking the BMP signaling inhibitor, Smad6, had enlarged or hyperplastic valves (Galvin *et al*., 2000), indicating that Smad6 may regulate BMP2R signaling required for cardiac valvulogenesis. These various results suggest a model in which valves fail to form with insufficient BMP signaling, but are hyperplastic when BMP signaling is unregulated. The enlarged valves of *EGFR*$^{-/-}$ and *HB-EGF*$^{-/-}$ mice are consistent with the hypothesis that EGFR, activated by HB-EGF, acts to downregulate BMP signaling in the developing valves. In the absence of either the ligand or its receptor, excessive BMP signaling leads to hyperproliferation. This hypothesis, which is consistent with the ability of EGFR to regulate BMP signaling in cell

culture (Kretzschmar *et al*., 1997; Nonaka *et al*., 1999), in part through phosphorylation and stabilization of the Smad transcriptional co-repressor TGIF (Lo *et al*., 2001), is supported by dramatic increases in cells staining positive for nuclear Smad1/5/8 in the hyperplastic *HB-EGF*$^{-/-}$ valves. To our knowledge, this is the first genetic evidence corroborating a physiological role for mammalian EGFR in transmodulating signaling by TGFβ superfamily members.

The similarities in heart as well as lung defects displayed by *HB-EGF*$^{-/-}$ and *TACE*$^{-/-}$ lines of mice strongly suggest that in addition to being a proTGFα convertase (Peschon *et al*., 1998; Sunnarborg *et al*., 2002), TACE is also a key regulator of HB-EGF shedding. The corollary of this conclusion is that soluble HB-EGF, not its integral membrane precursor, is required for normal valvulogenesis, although available reagents have not allowed us to confirm impaired shedding of endogenous HB-EGF from *TACE*$^{-/-}$ cells. However, recombinant TACE correctly cleaved a peptide substrate corresponding to the membrane-proximal cleavage site of proHB-EGF, and cotransfection of TACE enhanced the shedding of exogenous HB-EGF from *TACE*$^{-/-}$ fibroblasts (Sunnarborg *et al*., 2002). Hence, the combination of genetic, biochemical and cell biological evidence makes a compelling case for TACE as a physiological HB-EGF convertase. Other metalloproteases put forward as candidate HB-EGF convertases include MMP-3 (Suzuki *et al*., 1997; Bursi *et al*., 2002) and MMP-7/matrilysin (Yu *et al*., 2002), as well as the disintegrin metalloproteases ADAM9 (Izumi *et al*., 1998), ADAM10 (Lemjabbar and Basbaum, 2002; Yan *et al*., 2002) and ADAM12/meltrin α (Asakura *et al*., 2002). In particular, it was recently reported that GPCR-activated shedding of HB-EGF was blocked by a dominant-negative form of ADAM12, and that a metalloprotease inhibitor of HB-EGF shedding bound ADAM12 and inhibited hypertrophic changes in a mouse model (Asakura *et al*., 2002). However, although 30% of *ADAM12*$^{-/-}$ mice died prior to weaning, no heart defects were observed (Kurisaki *et al*., 2003). Conceivably, ADAM12 may have a role in induced but not constitutive shedding of HB-EGF.

Based on published reports as well as the findings reported here, it appears that all four ErbB receptors are required for normal heart development. Genetic evidence suggests that ErbB2 and ErbB4 form a NRG-1-activated heterodimer necessary for ventricular trabeculation (Gassmann *et al*., 1995; Lee *et al*., 1995; Erickson *et al*., 1997), and mice lacking any of these proteins die by E11.5. ErbB3, on the other hand, is essential for the formation of endocardial cushions, and *ErbB3*$^{-/-}$ mice frequently die in mid-gestation with abnormally small cushions (Erickson *et al*., 1997). In contrast, HB-EGF induced signaling by EGFR is required at a later stage for remodeling of the cardiac valves. The requirement for these related receptors at distinct stages of heart development is consistent with their observed ability to differentially activate various signaling pathways. An important, unanswered question is whether EGFR partners with another ErbB receptor to regulate valvulogenesis. The lack of valve defects in rescued ErbB4 hearts suggests that ErbB4 is not essential. The underdeveloped cushions of *ErbB3*$^{-/-}$ hearts, on the other hand, indicate that this receptor is required for an early step in valvulogenesis (Camenisch *et al*., 2002), but do not exclude a requirement for ErbB3, possibly in partnership with EGFR, in the later stage of valve remodeling. Future studies should be aimed at determining whether EGFR functions as a homo- or heterodimer in this context, as well as deciphering the respective mechanisms by which the four ErbB proteins regulate distinct stages of heart development.

Materials and methods

Reagents

B6EiC3H-*a/A-EGFR*$^{wa\text{-}2/wa\text{-}2}$*Wnt3a*^{vt} mice were from Jackson Laboratory (Bar Harbor, ME). *EGFR*$^{-/-}$ mice on a CD-1 or CD-1 × ALR.129 hybrid background were kindly provided by David Threadgill [University of North Carolina, Chapel Hill (UNC-CH)]. *TACE*$^{+/-}$ mice harboring the inactivating *TACE*$^{\Delta Zn}$ mutation (Peschon *et al*., 1998), a gift from Jacques Peschon and Roy Black (Immunex, Seattle, WA), were maintained on a C57BL/6J × 129/Sv hybrid background. Hearts from transgene rescued *ErbB4*$^{-/-}$ mice were kindly provided by Martin Gassmann (National Institute for Medical Research, London).

Gene targeting

HB-EGF and *BTC* genomic clones were isolated from a 129/Sv mouse lambda library (Stratagene, La Jolla, CA) using a mouse *HB-EGF* cDNA (kindly provided by Michael Klagsbrun, Harvard Medical School, Boston, MA) or *BTC* cDNA. Plasmid pNTK was used to construct targeting vectors as depicted in Figure 1; resulting constructs were electroporated into R1 ES cells (Luetteke *et al*., 1999). Correctly targeted, G418-resistant ES cell clones of normal karyotype were microinjected into 3.5-day-old C57BL/6J blastocysts, which were then implanted into pseudopregnant CD-1 foster mothers by the UNC-CH Animal Models Core. Chimeras transmitting to germline were crossed to C57BL/6J partners, and subsequent generations of mice maintained on a mixed C57BL/6J × 129/Sv background. PCR primer sequences used for genotyping are available upon request.

Organ harvest and analysis

Neonatal mice were killed by halothane inhalation; older mice were asphyxiated by CO_2 according to IACUC guidelines. Excised organs were fixed in 10% buffered formalin for 48–72 h prior to paraffin embedding. Histological sections (5 μm) were prepared by the UNC-CH Histopathology Core and stained as indicated. Antibodies for immunohistochemistry were as follows: anti-Ki67 (sc-7846), Santa Cruz Biotechnology, Santa Cruz, CA; anti-phospho-Smad1(Ser463/465)/Smad5(Ser463/465)/Smad8(Ser462/428) (9511), Cell Signaling Technology, Beverly, MA; and anti-prosurfactant protein C (SURFCPabr), Research Diagnostics, Flanders, NJ. Bound antibodies were visualized with the horseradish peroxidase-based ABC Staining System kit (Santa Cruz Biotechnology, Santa Cruz, CA) (Schroeder and Lee, 1998). Negative controls were obtained by incubating primary antibodies with excess peptide immunogens prior to immunostaining.

For analysis of heart development, timed matings were performed, with E0.5 defined as the morning of the day that the vaginal plug was first observed. At select gestational ages, dams were killed, and embryos removed and fixed in 4% paraformaldehyde for 48 h prior to paraffin embedding. Measurements of endocardial cushions and valves were performed on captured hematoxylin–eosin (H&E) images using the Bioquant software program in the UNC-CH Imaging Core (supported by NCI grant P30-CA16086). To assess cell proliferation, pregnant dams were injected with 100 μg/g body weight BrdU (Cell Proliferation Labeling Reagent, Amersham Biosciences Corp., Piscataway, NJ) 2 h prior to death. Heart sections were then stained with mouse BrdU monoclonal antibody (Dako, Carpinteria, CA). To assess apoptosis, TUNEL assays were performed on heart sections using the ApopTag Plus Peroxidase *in situ* Apoptosis Detection kit (Intergen, Purchase, NY). The ratios of BrdU- and TUNEL-positive cells to total cells in heart cushions were determined for two sections per sample and averaged for statistical analyses.

RNA analyses

RNA was isolated for northern blots using Trizol as directed (Invitrogen, Carlsbad, CA). Samples were probed (Luetteke *et al*., 1999) using cloned *HB-EGF* or *BTC* cDNAs. *In situ* hybridization analyses were performed

on paraffin sections using cDNA-derived antisense riboprobes as described (Luetteke *et al*., 1999; Kornblum *et al*., 2000). Sense riboprobes were hybridized for controls.

Echocardiography

Two-dimensional and M-mode imaging were performed using an ATL HDI 5000 ultrasound system equipped with a CL10-5 CVasc/mouse scan head (Philips Medical Systems, Andover, MA). Left ventricular end diastolic dimension (*LVEDD*) and end systolic dimension (*LVESD*), interventricular septum thickness (*IVST*) and posterior wall thickness (*PWT*) were obtained from M-mode tracings. All LV dimension data are presented as the average of two measurements. The percentage of fractional shortening (%SF) was calculated from the equation:

$$\%SF = (LVEDD - LVESD)/LVEDD \times 100.$$

Statistical analysis

Statistical analyses were performed by UNC Lineberger Comprehensive Cancer Center Biostatistics Core using SAS statistical software (Version 8.2; SAS Institute, Cary, NC). Exact *P* values were calculated for all two-group comparisons using the non-parametric Wilcoxon two-group test.

Acknowledgements

We thank Benjamin Neel, Jacques Peschon, Noreen Luetteke and Julian Moiseiwitsch for their advice, and Paivi Miettinen for analysis of pancreata. We also thank Virginia Godfrey for help in analyzing pathologies, Nolan Yeung for performing the *in situ* hybridizations, Wuhan Jiang for preparing heart sections, and Robert Schoonhoven and Dominic Moore, respectively, for assistance with cushion/valve measurements and statistical analyses. This work was supported by NIH grants CA43793, CA61896 and CA85410 (D.C.L.), AG021096 and HL65619 (C.P.) and USAMRMC grant DAMD17 (L.F.J.).

References

Arkonac,B.M., Foster,L.C., Sibinga,N.E., Patterson,C., Lai,K., Tsai,J.C., Lee,M.E., Perrella,M.A. and Haber,E. (1998) Vascular endothelial growth factor induces heparin-binding epidermal growth factor-like growth factor in vascular endothelial cells. *J. Biol. Chem.*, **273**, 4400–4405.

Asakura,M. *et al*. (2002) Cardiac hypertrophy is inhibited by antagonism of ADAM12 processing of HB-EGF: metalloproteinase inhibitors as a new therapy. *Nat. Med.*, **8**, 35–40.

Bartram,U., Bartelings,M.M., Kramer,H.H. and Gittenberger-de Groot, A.C. (2001) Congenital polyvalvular disease: a review. *Pediatr. Cardiol.*, **22**, 93–101.

Beerli,R.R. and Hynes,N.E. (1996) Epidermal growth factor-related peptides activate distinct subsets of ErbB receptors and differ in their biological activities. *J. Biol. Chem.*, **271**, 6071–6076.

Besner,G., Higashiyama,S. and Klagsbrun,M. (1990) Isolation and characterization of a macrophage-derived heparin-binding growth factor. *Cell Regul.*, **1**, 811–819.

Bursi,R., Sawa,M., Hiramatsu,Y. and Kondo,H. (2002) A three-dimensional quantitative structure–activity relationship study of heparin-binding epidermal growth factor shedding inhibitors using comparative molecular field analysis. *J. Med. Chem.*, **45**, 781–788.

Camenisch,T.D., Schroeder,J.A., Bradley,J., Klewer,S.E. and McDonald,J.A. (2002) Heart-valve mesenchyme formation is dependent on hyaluronan-augmented activation of ErbB2 ErbB3 receptors. *Nat. Med.*, **8**, 850–855.

Chen,B. *et al*. (2000) Mice mutant for Egfr and Shp2 have defective cardiac semilunar valvulogenesis. *Nat. Genet.*, **24**, 296–299.

Chien,K.R. (2000) Genomic circuits and the integrative biology of cardiac diseases. *Nature*, **407**, 227–232.

Clark,T.G., Conway,S.J., Scott,I.C., Labosky,P.A., Winnier,G., Bundy,J., Hogan,B.L. and Greenspan,D.S. (1999) The mammalian Tolloid-like 1 gene, *Tll1*, is necessary for normal septation and positioning of the heart. *Development*, **126**, 2631–2642.

Das,S.K., Wang,X.N., Paria,B.C., Damm,D., Abraham,J.A., Klagsbrun,M., Andrews,G.K. and Dey,S.K. (1994) Heparin-binding EGF-like growth factor gene is induced in the mouse uterus temporally by the blastocyst solely at the site of its apposition: a possible ligand for interaction with blastocyst EGF-receptor in implantation. *Development*, **120**, 1071–1083.

Das,S.K., Das,N., Wang,J., Lim,H., Schryver,B., Plowman,G.D. and Dey,S.K. (1997) Expression of betacellulin and epiregulin genes in the mouse uterus temporally by the blastocyst solely at the site of its apposition is coincident with the 'window' of implantation. *Dev. Biol.*, **190**, 178–190.

Delot,E.C., Bahamonde,M.E., Zhao,M. and Lyons,K.M. (2003) BMP signaling is required for septation of the outflow tract of the mammalian heart. *Development*, **130**, 209–220.

Demeterco,C., Beattie,G.M., Dib,S.A., Lopez,A.D. and Hayek,A. (2000) A role for activin A and betacellulin in human fetal pancreatic cell differentiation and growth. *J. Clin. Endocrinol. Metab.*, **85**, 3892–3897.

Dunbar,A.J. and Goddard,C. (2000) Structure–function and biological role of betacellulin. *Int. J. Biochem. Cell Biol.*, **32**, 805–815.

Eisenberg,L.M. and Markwald,R.R. (1995) Molecular regulation of atrioventricular valvuloseptal morphogenesis. *Circ. Res.*, **77**, 1–6.

Elenius,K., Corfas,G., Paul,S., Choi,C.J., Rio,C., Plowman,G.D. and Klagsbrun,M. (1997) A novel juxtamembrane domain isoform of HER4/ErbB4. Isoform-specific tissue distribution and differential processing in response to phorbol ester. *J. Biol. Chem.*, **272**, 26761–26768.

Erickson,S.L., O'Shea,K.S., Ghaboosi,N., Loverro,L., Frantz,G., Bauer,M., Lu,L.H. and Moore,M.W. (1997) ErbB3 is required for normal cerebellar and cardiac development: a comparison with ErbB2- and heregulin-deficient mice. *Development*, **124**, 4999–5011.

Galvin,K.M. *et al*. (2000) A role for smad6 in development and homeostasis of the cardiovascular system. *Nat. Genet.*, **24**, 171–174.

Gassmann,M., Casagranda,F., Orioli,D., Simon,H., Lai,C., Klein,R. and Lemke,G. (1995) Aberrant neural and cardiac development in mice lacking the ErbB4 neuregulin receptor. *Nature*, **378**, 390–394.

Gaussin,V., Van de Putte,T., Mishina,Y., Hanks,M.C., Zwijsen,A., Huylebroeck,D., Behringer,R.R. and Schneider,M.D. (2002) Endocardial cushion and myocardial defects after cardiac myocyte-specific conditional deletion of the bone morphogenetic protein receptor ALK3. *Proc. Natl Acad. Sci. USA*, **99**, 2878–2883.

Graus-Porta,D., Beerli,R.R., Daly,J.M. and Hynes,N.E. (1997) ErbB-2, the preferred heterodimerization partner of all ErbB receptors, is a mediator of lateral signaling. *EMBO J.*, **16**, 1647–1655.

Higashiyama,S., Abraham,J.A., Miller,J., Fiddes,J.C. and Klagsbrun,M. (1991) A heparin-binding growth factor secreted by macrophage-like cells that is related to EGF. *Science*, **251**, 936–939.

Iwamoto,R. and Mekada,E. (2000) Heparin-binding EGF-like growth factor: a juxtacrine growth factor. *Cytokine Growth Factor Rev.*, **11**, 335–344.

Iwamoto,R., Handa,K. and Mekada,E. (1999) Contact-dependent growth inhibition and apoptosis of epidermal growth factor (EGF) receptor-expressing cells by the membrane-anchored form of heparin-binding EGF-like growth factor. *J. Biol. Chem.*, **274**, 25906–25912.

Izumi,Y. *et al*. (1998) A metalloprotease-disintegrin, MDC9/meltrin-γ/ADAM9 and PKCδ are involved in TPA-induced ectodomain shedding of membrane-anchored heparin-binding EGF-like growth factor. *EMBO J.*, **17**, 7260–7272.

Jiang,X., Rowitch,D.H., Soriano,P., McMahon,A.P. and Sucov,H.M. (2000) Fate of the mammalian cardiac neural crest. *Development*, **127**, 1607–1616.

Kallincos,N.C., Xian,C.J., Dunbar,A.J., Couper,R.T. and Read,L.C. (2000) Cloning of rat betacellulin and characterization of its expression in the gastrointestinal tract. *Growth Factors*, **18**, 203–213.

Kennedy,T.G., Brown,K.D. and Vaughan,T.J. (1993) Expression of the genes for the epidermal growth factor receptor and its ligands in porcine corpora lutea. *Endocrinology*, **132**, 1857–1859.

Kim,R.Y., Robertson,E.J. and Solloway,M.J. (2001) Bmp6 and Bmp7 are required for cushion formation and septation in the developing mouse heart. *Dev. Biol.*, **235**, 449–466.

Kornblum,H.I., Yanni,D.S., Easterday,M.C. and Seroogy,K.B. (2000) Expression of the EGF receptor family members ErbB2, ErbB3, and ErbB4 in germinal zones of the developing brain and in neurosphere cultures containing CNS stem cells. *Dev. Neurosci.*, **22**, 16–24.

Kretzschmar,M., Doody,J. and Massague,J. (1997) Opposing BMP and EGF signalling pathways converge on the TGF-β family mediator Smad1. *Nature*, **389**, 618–622.

Kurisaki,T. *et al*. (2003) Phenotypic analysis of Meltrin α (ADAM12)-deficient mice: involvement of Meltrin α in adipogenesis and myogenesis. *Mol. Cell. Biol.*, **23**, 55–61.

Lakkis,M.M. and Epstein,J.A. (1998) Neurofibromin modulation of ras activity is required for normal endocardial–mesenchymal transformation in the developing heart. *Development*, **125**, 4359–4367.

Lamers,W.H., Viragh,S., Wessels,A., Moorman,A.F. and Anderson,R.H.

(1995) Formation of the tricuspid valve in the human heart. *Circulation*, **91**, 111–121.

Lee,K.F., Simon,H., Chen,H., Bates,B., Hung,M.C. and Hauser,C. (1995) Requirement for neuregulin receptor erbB2 in neural and cardiac development. *Nature*, **378**, 394–398.

Lemjabbar,H. and Basbaum,C. (2002) Platelet-activating factor receptor and ADAM10 mediate responses to *Staphylococcus aureus* in epithelial cells. *Nat. Med.*, **8**, 41–46.

Lo,R.S., Wotton,D. and Massague,J. (2001) Epidermal growth factor signaling via Ras controls the Smad transcriptional co-repressor TGIF. *EMBO J.*, **20**, 128–136.

Luetteke,N.C., Qiu,T.H., Peiffer,R.L., Oliver,P., Smithies,O. and Lee,D.C. (1993) TGF α deficiency results in hair follicle and eye abnormalities in targeted and waved-1 mice. *Cell*, **73**, 263–278.

Luetteke,N.C., Qiu,T.H., Fenton,S.E., Troyer,K.L., Riedel,R.F., Chang,A. and Lee,D.C. (1999) Targeted inactivation of the EGF and amphiregulin genes reveals distinct roles for EGF receptor ligands in mouse mammary gland development. *Development*, **126**, 2739–2750.

Mashima,H., Ohnishi,H., Wakabayashi,K., Mine,T., Miyagawa,J., Hanafusa,T., Seno,M., Yamada,H. and Kojima,I. (1996) Betacellulin and activin A coordinately convert amylase-secreting pancreatic AR42J cells into insulin-secreting cells. *J. Clin. Invest.*, **97**, 1647–1654.

Mashima,H., Yamada,S., Tajima,T., Seno,M., Yamada,H., Takeda,J. and Kojima,I. (1999) Genes expressed during the differentiation of pancreatic AR42J cells into insulin-secreting cells. *Diabetes*, **48**, 304–309.

Meyer,D. and Birchmeier,C. (1995) Multiple essential functions of neuregulin in development. *Nature*, **378**, 386–390.

Miettinen,P.J., Berger,J.E., Meneses,J., Phung,Y., Pedersen,R.A., Werb,Z. and Derynck,R. (1995) Epithelial immaturity and multiorgan failure in mice lacking epidermal growth factor receptor. *Nature*, **376**, 337–341.

Miettinen,P.J. *et al*. (1997) Impaired lung branching morphogenesis in the absence of functional EGF receptor. *Dev. Biol.*, **186**, 224–236.

Mohler,E.R.,III, Gannon,F., Reynolds,C., Zimmerman,R., Keane,M.G. and Kaplan,F.S. (2001) Bone formation and inflammation in cardiac valves. *Circulation*, **103**, 1522–1528.

Naglich,J.G., Metherall,J.E., Russell,D.W. and Eidels,L. (1992) Expression cloning of a diphtheria toxin receptor: identity with a heparin-binding EGF-like growth factor precursor. *Cell*, **69**, 1051–1061.

Nonaka,K., Shum,L., Takahashi,I., Takahashi,K., Ikura,T., Dashner,R., Nuckolls,G.H. and Slavkin,H.C. (1999) Convergence of the BMP and EGF signaling pathways on Smad1 in the regulation of chondrogenesis. *Int. J. Dev. Biol.*, **43**, 795–807.

Peschon,J.J. *et al*. (1998) An essential role for ectodomain shedding in mammalian development. *Science*, **282**, 1281–1284.

Prenzel,N., Zwick,E., Daub,H., Leserer,M., Abraham,R., Wallasch,C. and Ullrich,A. (1999) EGF receptor transactivation by G-protein-coupled receptors requires metalloproteinase cleavage of proHB-EGF. *Nature*, **402**, 884–888.

Raab,G. and Klagsbrun,M. (1997) Heparin-binding EGF-like growth factor. *Biochim. Biophys. Acta*, **1333**, F179–F199.

Riese,D.J.,II and Stern,D.F. (1998) Specificity within the EGF family/ErbB receptor family signaling network. *BioEssays*, **20**, 41–48.

Riese,D.J.,II, Bermingham,Y., van Raaij,T.M., Buckley,S., Plowman,G.D. and Stern,D.F. (1996a) Betacellulin activates the epidermal growth factor receptor and erbB-4, and induces cellular response patterns distinct from those stimulated by epidermal growth factor or neuregulin-β. *Oncogene*, **12**, 345–353.

Riese,D.J., Kim,E.D., Elenius,K., Buckley,S., Klagsbrun,M., Plowman,G.D. and Stern,D.F. (1996b) The epidermal growth factor receptor couples transforming growth factor-α, heparin-binding epidermal growth factor-like factor, and amphiregulin to Neu, ErbB-3, and ErbB-4. *J. Biol. Chem.*, **271**, 20047–20052.

Sasada,R., Ono,Y., Taniyama,Y., Shing,Y., Folkman,J. and Igarashi,K. (1993) Cloning and expression of cDNA encoding human betacellulin, a new member of the EGF family. *Biochem. Biophys. Res. Commun.*, **190**, 1173–1179.

Schroeder,J.A. and Lee,D.C. (1998) Dynamic expression and activation of ERBB receptors in the developing mouse mammary gland. *Cell Growth Differ.*, **9**, 451–464.

Shing,Y., Christofori,G., Hanahan,D., Ono,Y., Sasada,R., Igarashi,K. and Folkman,J. (1993) Betacellulin: a mitogen from pancreatic β cell tumors. *Science*, **259**, 1604–1607.

Sibilia,M. and Wagner,E.F. (1995) Strain-dependent epithelial defects in mice lacking the EGF receptor. *Science*, **269**, 234–238.

Sibilia,M., Steinbach,J.P., Stingl,L., Aguzzi,A. and Wagner,E.F. (1998) A strain-independent postnatal neurodegeneration in mice lacking the EGF receptor. *EMBO J.*, **17**, 719–731.

Srivastava,D. and Olson,E.N. (2000) A genetic blueprint for cardiac development. *Nature*, **407**, 221–226.

Strachan,L., Murison,J.G., Prestidge,R.L., Sleeman,M.A., Watson,J.D. and Kumble,K.D. (2001) Cloning and biological activity of epigen, a novel member of the epidermal growth factor superfamily. *J. Biol. Chem.*, **276**, 18265–18271.

Sunnarborg,S.W. *et al*. (2002) Tumor necrosis factor-α converting enzyme (TACE) regulates epidermal growth factor receptor ligand availability. *J. Biol. Chem.*, **277**, 12838–12845.

Suzuki,M., Raab,G., Moses,M.A., Fernandez,C.A. and Klagsbrun,M. (1997) Matrix metalloproteinase-3 releases active heparin-binding EGF-like growth factor by cleavage at a specific juxtamembrane site. *J. Biol. Chem.*, **272**, 31730–31737.

Tamura,R. *et al*. (2001) Immunohistochemical localization of betacellulin, a member of epidermal growth factor family, in atherosclerotic plaques of human aorta. *Atherosclerosis*, **155**, 413–423.

Threadgill,D.W. *et al*. (1995) Targeted disruption of mouse EGF receptor: effect of genetic background on mutant phenotype. *Science*, **269**, 230–234.

Tidcombe,H., Mathers,K. and Gassmann,M. (2001) Genetic rescue of cardiac defects in mice lacking the neuregulin receptor ErbB4. Fourteenth International Congress of Development Biology, July 2001. *Dev.. Growth Differ.*, **43(Suppl.)**, S8–S88.

Troyer,K.L., Luetteke,N.C., Saxon,M.L., Qiu,T.H., Xian,C.J. and Lee,D.C. (2001) Growth retardation, duodenal lesions, and aberrant ileum architecture in triple null mice lacking EGF, amphiregulin, and TGF-α. *Gastroenterology*, **121**, 68–78.

Yamamoto,K. *et al*. (2000) Recombinant human betacellulin promotes the neogenesis of β-cells and ameliorates glucose intolerance in mice with diabetes induced by selective alloxan perfusion. *Diabetes*, **49**, 2021–2027.

Yan,Y., Shirakabe,K. and Werb,Z. (2002) The metalloprotease Kuzbanian (ADAM10) mediates the transactivation of EGF receptor by G protein-coupled receptors. *J. Cell Biol.*, **158**, 221–226.

Yoshizumi,M., Kourembanas,S., Temizer,D.H., Cambria,R.P., Quertermous,T. and Lee,M.E. (1992) Tumor necrosis factor increases transcription of the heparin-binding epidermal growth factor-like growth factor gene in vascular endothelial cells. *J. Biol. Chem.*, **267**, 9467–9469.

Yu,W.H., Woessner,J.F.,Jr, McNeish,J.D. and Stamenkovic,I. (2002) CD44 anchors the assembly of matrilysin/MMP-7 with heparin-binding epidermal growth factor precursor and ErbB4 and regulates female reproductive organ remodeling. *Genes Dev.*, **16**, 307–323.

Zhao,J., Chen,H., Peschon,J.J., Shi,W., Zhang,Y., Frank,S.J. and Warburton,D. (2001) Pulmonary hypoplasia in mice lacking tumor necrosis factor-α converting enzyme indicates an indispensable role for cell surface protein shedding during embryonic lung branching morphogenesis. *Dev. Biol.*, **232**, 204–218.

Received August 16, 2002; revised March 13, 2003; accepted April 4, 2003